eppendorf

Impress Yourself

The new Eppendorf Cell Culture Consumables

The all new line of Eppendorf Cell Culture Consumables will truly delight your cells. The outstanding design, reliability and purity is based on more than 50 years of experience. Products created by experts, developed for perfectionists. Impress yourself!

> Unsurpassed quality, clarity, purity and sterility, providing reliable cell culture conditions
> Significantly improved design for more safety and consistency
> Maximum safety and confidence during storage and transportation

ccc.eppendorf.com • 800-645-3050

STEM CELLS®
Original Article

Modeling Stem Cell Population Growth: Incorporating Terms for Proliferative Heterogeneity

B.M. DEASY,[a,b] R.J. JANKOWSKI,[a,b] T.R. PAYNE,[a,b] B. CAO,[a,b] J.P. GOFF,[c] J.S. GREENBERGER,[c] J. HUARD[a,b]

[a]Departments of Orthopaedic Surgery, Molecular Genetics, Biochemistry and Bioengineering, University of Pittsburgh School of Medicine; [b]Growth and Development Laboratory, Children's Hospital of Pittsburgh; [c]Department of Radiation Oncology, University of Pittsburgh School of Medicine, Pittsburgh, Pennsylvania, USA

Key Words. *Nonexponential · Mathematical model · Kinetics · Muscle-derived stem cell · Proliferation*

ABSTRACT

Expansion of the undifferentiated stem cell phenotype is one of the most challenging aspects in stem cell research. Clinical protocols for stem cell therapeutics will require standardization of defined culture conditions. A first step in the development of predictable and reproducible, scalable bioreactor processes is the development of mathematical growth models. This paper provides practical models for describing cell growth in general, which are particularly well suited for examining stem cell populations. The nonexponential kinetics of stem cells derive from proliferative heterogeneity, which is biologically recognized as mitosis, quiescence, senescence, differentiation, or death. Here, we examined the assumptions of the *Sherley* model, which describes heterogeneous expansion in the absence of cell loss. We next incorporated terms into the model to account for A) cell loss or apoptosis and B) cell differentiation. We conclude that the basic assumptions of the model are valid and a high correlation between the modified equations and experimental data obtained using muscle-derived stem cells was observed. Finally, we demonstrate an improved estimation of the kinetic parameters. This study contributes to both the biological and mathematical understanding of stem cell dynamics. Further, it is expected that the models will prove useful in establishing standardization of cell culture conditions and scalable systems and will be required to develop clinical protocols for stem cell therapeutics. *Stem Cells 2003;21:536-545*

INTRODUCTION

Stem cell utilization in regenerative medicine and cell-based therapies offers immense potential. Key to advancing these efforts is the development of systems to expand cells to clinically relevant numbers [1-5] while maintaining the desired stem cell phenotype. The systems will rely on a sufficient understanding and control of the basic mechanisms involved in the determination of stem cell fate, in particular, the choice between self-renewal and differentiation. Also important, it is necessary to quantitatively assess the status of the expanding population. Mathematical growth models will play a key role in developing such systems, as they can be both predictive tools for expansion potential and tools to characterize and measure current kinetic parameters of a stem cell population.

The development of a population growth model constitutes one step toward understanding the dynamics of stem

Correspondence: Johnny Huard, Ph.D., Growth and Development Laboratory, Children's Hospital of Pittsburgh; Departments of Orthopedic Surgery, Molecular Genetics, Biochemistry, and Bioengineering, University of Pittsburgh School of Medicine, Pittsburgh, Pennsylvania 15213, USA. Telephone: 412-692-8148; Fax: 412-692-7095; e-mail: jhuard@pitt.edu *Received February 18, 2003; accepted for publication May 8, 2003.*

cell population growth. The multiple stem cell fates are regulated by both intrinsic and extrinsic controls. Differential intercellular localization and inheritance of molecular determinants result in asymmetric daughter cells [6-9]. In addition, the stem cell niche or microenvironment, consisting of extracellular matrix including integrins, cytokines, and various cell types, differentially stimulates stem cells to express alternative phenotypes [10-13]. While efforts to biologically understand these controls develop, mathematical models are also necessary.

Proliferative heterogeneity is the key characteristic of stem cell populations and must be incorporated into models. While asynchronous exponential growth often is used to model cell population dynamics, few cell populations behave in this way in vitro [14-17] or in vivo [18, 19]. Even tumorigenic cells behave nonexponentially [20-23]. Nonexponential growth is the result of nondividing cells present in the population. Biologically, the nondividing nature of these cells is attributable to quiescence, terminal differentiation, senescence, or cell death (Fig. 1), while mathematically it translates to a growth fraction, α, which is <1, and/or a death rate, μ, which is >0. Thus the population size at time t, N (t), depends directly on A) the birth rate (which is a function of the cell cycle time); B) the growth or mitotically active fraction, and C) the death rate. Mathematical models designed to describe nonexponential growth are the result of variations on these three themes.

Early models of nonexponential growth recognized that it was necessary to account for the "lakes" of necrotic cells observed in the core of tumors [24, 25]. Tumor growth does not continue on an exponential path; rather, it reaches a plateau as cell death removes proliferating cells from the population [18]. Many of the early, ad hoc models used Gompertz or logistic distributions to describe the *S*-shaped curve [26, 27], which was typically due to space and nutrient deprivation. *Gyllenberg* and *Webb* [27] explained the Gompertzian tumor growth curves by using parameters to represent the rates of cells transitioning reversibly between the proliferative and quiescent states as a function of tumor size, thereby incorporating variable growth fraction. Reducing the number of model parameters, *Izquierdo* and *Perez* [28] described the quiescent or nonproliferating component as proliferating cells with "long" division times and a birth rate equal to 1. Other models have used the theory of age-dependent branching processes to account for changes in growth fraction or changes in cell division rate associated with cell age [29-31]. In a similar vein, *Hayflick's* hypothesis of limited cellular lifespan may be incorporated into models as a finite number of divisions [32] or a decreased doubling rate associated with time [33], such that cellular senescence is consequently modeled as a change in growth fraction. Even contact-inhibited cell growth has been modeled by including terms to describe the probability of a cell dividing as dependent on its position in 1-, 2-, or 3-dimensional space [34], such that the proliferation rate, specifically the growth fraction, decreases as N increases and cells occupy more space.

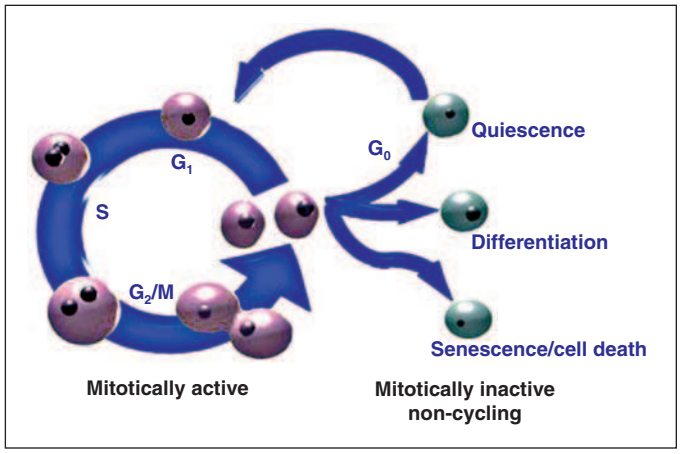

Figure 1. Nonlinear growth is the result of nondividing cells present in the population. *Schematic diagram illustrating the nondividing cellular states of quiescence (G_0), terminal differentiation, apoptosis/senescence. In this scenario, cells progress through the cycle and divide into daughter cells, which may begin a new mitotic cycle. Alternatively, the daughter cells may temporarily enter the dormant G_0 state or become terminally differentiated or exit the cycle to become senescent or apoptotic.*

The *Sherley* model [35], based on difference equations, demonstrates growth of populations with asymmetric divisions that result in dividing cells and quiescent or senescent cells. This model is particularly well suited for studying the expansion of all cell populations, as it does not make the logistic assumption of a saturation density that is associated with age or space-nutrient depletion. Stem cells require specific culture conditions to maintain the stem cell phenotype or self-renewing divisions; such populations often are maintained at a density well below any culture-induced carrying capacity. The *Sherley* model can be used to describe growth in "unrestricted" conditions. In addition to predicting long-term expansion, it provides useful parameters to describe the current behavior of the population. This model can be used to estimate division time, mitotic fraction, or population doubling time, and therefore enables researchers to assess the behavior of a particular cell population under various culture conditions.

In this study we evaluate the assumptions of the *Sherley* model. We then augment the *Sherley* model by incorporating terms to account for the alternative stem cell fates of apoptosis and differentiation. We offer two modified models for cell growth in the presence of cell loss or cell differentiation. Using muscle-derived stem cells (MDSCs)

induced to apoptose or to undergo myogenic differentiation, we observed good fits in the presence of these events.

Materials and Methods

Assumptions of Nonlinear, Nonexponential Population Growth

Population growth and estimations of proliferation parameters often are calculated using the exponential equation: $N = N_0\, 2^{t/DT}$ where the number of cells, N, at time, t, depends solely on the initial number of cells, N_0, and its division time, DT; this equation assumes that all cells are actively dividing to give rise to two daughter cells. In order to more accurately describe the dynamics, the *Sherley* model [35] includes a parameter that accounts for the presence of nondividing cells:

$$N = N_0 \left[0.5 + \frac{1 - (2\alpha)^{(t/DT)+1}}{2(1 - 2\alpha)} \right] \qquad (1)$$

Previously, we have used this model to describe cell expansion occurring with negligible cell loss [36, 37], where α is the mitotic fraction and DT is the division time (F_D and GT, respectively, in *Sherley et al.* [35]). In the first part of this study, we verified three primary assumptions of this model, namely that A) the DT is constant; B) dividing cells are capable of giving rise to both dividing and nondividing cells, and C) nondividing cells do not re-enter the cell cycle during the observed period.

MDSCs were obtained as previously described [38-40]. The cells used in this study derive from a single clone (termed MC13), and we have previously observed that early passage cells of this clone have proliferation characteristics similar to those of primary populations in normal growth conditions [36]. Cells were plated on collagen-coated flasks at 225 cells/cm^2 with normal culture medium containing 10% fetal calf serum (FCS), 10% horse serum (HS), 0.5% chick embryo extract (CEE), and 1% penicillin/streptomycin in Dulbecco's modified Eagle's medium (DMEM, GIBCO; Carlsbad, CA; http://www.lifetech.com).

To test if DT is constant in the confluency range of 10%-50%, a microscopic imaging system was used [36, 37]. Time-lapsed videos consisted of images acquired every 10 minutes for a period of 5 days. DT of the dividing cells (n = 75-100) was measured as the lapsed time between cytokinetic events. Division times were determined for each day, according to the day on which the cycle began. It should be noted that this method has a slight bias toward shorter division times. As the ability to track cells decreases with time, cells with longer DT are more likely to be lost in the growing crowd, i.e., it becomes more difficult to visually track cells as confluency increases. Therefore, while we recorded the video for 5-6 days, the DTs were measured for cells that initiated their cycles on days 1, 2, and 3. Three replicate experiments were performed. The distribution of DTs was compared among the various days using Kruskal-Wallis one-way analysis of variance on ranks.

To verify that dividing cells are capable of giving rise to both dividing and nondividing cells, we first defined a nondividing cell as one that did not divide in three times the median division time. Next, we directly observed the time-lapsed images for asymmetric divisions and constructed cellular division lineage trees.

Derivation of the Population Growth Model with Cell Loss

In this model, population size, N(t), depends on three parameters: A) the DT, B) the mitotic fraction (α), and C) cell loss due to cell mortality or migration, M(t). In the absence of this third term, M(t), the model is insufficient to describe population growth under conditions of significant cell loss. In this derivation, N and M are functions of time, while DT and α are constants. As in *Sherley et al.* [35, 36], letting N be the number of live cells at time t and M be the cumulative number of dead or lost cells at time t, a series of discrete equations results in

$$N_i = (1-\alpha)(2\alpha)^0 N_0 + (1-\alpha)(2\alpha)^1 (N_0) + (1-\alpha)(2\alpha)^2 (N_0) + \ldots + (1-\alpha)(2\alpha)^{i-1} (N_0) + (2\alpha)^i (N_0) - M_i$$

Expanding and rearranging the terms reveals a geometric series that simplifies to

$$N_i = N_0 \left[0.5 + 0.5 \sum_0^n (2\alpha)^i \right] - M_i$$

where i = any positive value t/DT, N_i = the number of live cells at time t, M_i = the cumulative number of dead cells at time t, and N_0 = the initial number of cells.

Applying the identity,

$$a \sum_{i=0}^{n} x^i = a \frac{1 - x^{n+1}}{1 - x}$$

then provides the model equation for growth with cell loss:

$$N = N_0 \left[0.5 + \frac{1 - (2\alpha)^{(t/DT)+1}}{2(1 - 2\alpha)} \right] - M \qquad (2)$$

The last term, M, which is new to this equation, enables a more accurate prediction of α under conditions of substantive cell loss. In the absence of this term, the mitotic fraction is underestimated, as the total number of cells generated appears lower than in actuality.

To test the validity and applicability of this model, MDSCs were plated on 6-well collagen-coated plates at a density of 225 cells/cm^2 in normal growth medium, as described above. The average number of cells in each view-field on day 0 was ~4. Cell death or apoptosis was induced

using the transcription inhibitor actinomycin D (AD) (0.5 ng/ml, Sigma; http://www.sigmaaldrich.com), which previously has been demonstrated to activate the caspase cascade [41, 42]. Images of population growth were acquired every 10 minutes for a 5-day period. From the video record, the live cell count, N(t), was determined at 12-hour intervals and DTs were measured as described above. Growth curves were normalized to $N_0 = 225$ cells/cm^2. Cell loss due to cell death was measured by continuous viewing of the video record. Cell death was recognized as a series of events including A) cessation of movement; B) cell blebbing, shrinkage, or bursting; C) change in phase contrast due to compromised membrane, and finally, D) cell detachment from the substratum. Apoptotic activity was confirmed by immunocytochemistry with anti-caspase-3 antibody (1:250, Zymed; San Francisco, CA; http://www.zymed.com). Mitotic activity was observed by 5-bromo-2′-deoxyuridine (BrdU) incorporation using biotinylated mouse anti-BrdU (1:250, Zymed), streptavidin-488 (1:1,000, Sigma), and Hoechst 33258 (0.01 mg/ml, Sigma). The number of dead cells measured during the interval t = 0 to t =12 hours was recorded as M (t = 12 hours). Accordingly, M (t = 24 hours) was determined as M (t = 12 hours) plus the number of dead cells measured during the interval t = 12 to t = 24 hours. In this way, all experimental data were determined from the same experiment. The population growth data (N_i and M_i) and DT then were curve-fit to equation (2) using nonlinear regression (Sigma Stat 2.0, Jandel Scientific; San Rafael, CA) to determine the r^2 Pearson product-moment coefficient of determination and to estimate α. Three replicate experiments were performed; α parameters were compared using Student's *t*-test.

Derivation of the Population Growth Model with Differentiation

In stem cell population growth there is a dynamic balance between self-renewal and differentiation processes. Such populations are rarely homogeneous in vitro, as the stem cell has a tendency, in response to a variety of signals, to give rise to precursor and fully differentiated cell types, while at the same time maintaining its reserve self. To provide a mathematical model for this cell growth and to understand these processes, we must include a term to account for nondividing, terminally differentiated cells. A term accounting for them may be added to equation (1) or (2) in the exact same way that the cell loss term was added earlier. Essentially, the number of live cells, N, consists of three subpopulations: A) the self-renewing cells ($N^{\text{Self-Renewing}}$); B) the mitotically active precursor cells, ($N^{\text{Precursor}}$), and C) the terminally differentiated cells, ($N^{\text{Differentiated}}$), such that

$$N = N^{\text{Self-Renewing}} + N^{\text{Precursor}} + N^{\text{Differentiated}}$$

To simplify, we say that the first two compartments are made up of proliferating cells while the third compartment represents nondividing cells. Thus we can write

$$N = N^{\text{Proliferating}} + N^{\text{Differentiated}}$$

or

$$N^{\text{Proliferating}} + N^{\text{Differentiated}} = N_0 \left[0.5 + \frac{1 - (2\alpha)^{(t/DT)+1}}{2(1 - 2\alpha)} \right] - M \quad (3)$$

To validate the growth model containing the term accounting for differentiation, we examined the population growth kinetics of myogenic cells under differentiation-inducing conditions. In the unique case of myogenic differentiation, several mononuclear cells fuse together to form multinucleated myotubes that morphologically denote the terminally differentiated state. The mononuclear population is mitotically active and consists of both self-renewing MDSCs and myogenic precursor cells. The total number of cells that have fused to become terminally differentiated myotubes is equal to the total number of nuclei in all of the myotubes. In essence, growth modeling in this way becomes an exercise in nuclei counting. In the specific case of stem cell growth with myogenic differentiation, we can substitute $N^{\text{Proliferating}} = N^{\text{Mononuclear}}$, and $N^{\text{Differentiated}} = N^{\text{FusedNuclei}}$, into equation (3) to obtain:

$$N^{\text{Mononuclear}} + N^{\text{FusedNuclei}} = N_0 \left[0.5 + \frac{1 - (2\alpha)^{(t/DT)+1}}{2(1 - 2\alpha)} \right] - M \quad (3.1)$$

To induce differentiation, MDSCs first were plated at a density of 1,000 cells/cm^2 on collagen-coated flasks in normal medium for 48 hours, then were cultured for 96 hours with 2.5% serum medium containing 1.25% HS, 1.25% FCS, 0.5% CEE, and 1% penicillin/streptomycin in DMEM. Population growth was recorded using the microscopic imaging system. The average number of cells per viewfield was 12 and growth curves were normalized to $N_0 = 1{,}000$ cells/cm^2. This video was used to determine $N^{\text{Mononuclear}}$, $N^{\text{FusedNuclei}}$, and DT. Proliferation and differentiation were confirmed by immunocytochemical staining performed at 24-hour intervals with anti-BrdU and anti-myosin heavy chain (anti-MyHC, 1:250, Sigma), a marker for differentiated muscle cells. Nuclei were visualized using Hoechst labeling. The growth data then were curve-fit to the model to obtain the r^2 correlation coefficient for the nonlinear regression and an estimation of the mitotic fraction. As above, three replicate experiments were performed and α parameters were compared using Student's *t*-test.

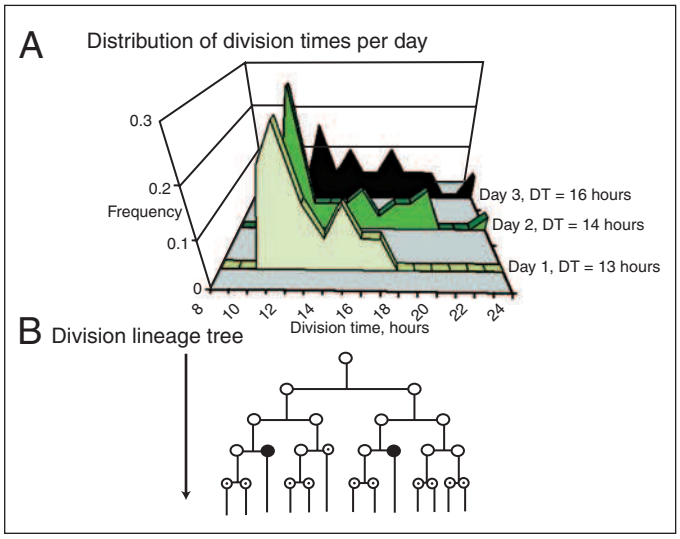

Figure 2. A) Median cell division time does not change significantly over the 3-day period (median = 15 hours, $p < 0.05$, Kruskal-Wallis one-way pairwise analysis of variance on ranks). *B) Typical cell division pedigree tree for MDSC. Asymmetric divisions are evident under normal growth conditions (20% serum medium); open circles (○) indicate mitotically active cells, closed circles (●) indicate nondividing cells, bulleted circles (⊙) indicate unknown fate.*

Results

Validation of Growth Model Assumptions

The distributions of cell cycle times observed during the 24-hour intervals were compared, and there were no statistical differences among the median division times (day-1 DT = 13 hours, day-2 DT = 14 hours, day-3 DT = 16 hours; $p = 0.411$). The distributions of DTs were skewed to the right with >90% of the cells dividing in the range of 10-24 hours. Indeed, fewer than 1% of the DTs were less than 10 hours, so the majority of the DTs outside of this range were >24 hours. The median cell cycle duration for the first 3 days was 15 hours. Although the statistical analysis revealed no significant difference among the days, there was a consistent trend toward increasing cell cycle time, with the distribution appearing to widen and shift toward longer times (Fig. 2A).

We also observed asymmetric divisions, which were recognized as cell divisions that gave rise to two daughter cells, one of which divided while the other did not. A representative division lineage tree that includes asymmetric divisions is shown in Figure 2B. As expected, the nondividing daughter cell generally underwent cell death or was observed to become quiescent (Fig. 2B); less frequently, the nondividing state was the result of differentiation, which was observed as cell fusion. It is important to note that the division lineage shown here (Fig. 2B) is not the typical type of division for the MDSC in normal culture condition. Rather, the majority of divisions are symmetric divisions. In addition, the model assumption that states that nondividing cells remain as nondividing cells and do not re-enter the cell cycle in the observed period was supported by our finding of a minority of cells that were present at the initiation of the video and underwent no division in the 5-day period. We also observed, as illustrated in Figure 2B, the presence of nondividing subpopulations, which result from dividing cells that remain quiescent or mitotically inactive for >45 hours. These findings validate the assumptions for equation derivation.

Validation of Growth Model with Cell Loss

Cell death was significantly increased in populations treated with AD, and we observed that this effect increased in a dose-dependent manner. In order to test the applicability of this model, we selected the dose of 0.5 ng/ml AD, which permitted cell division while also inducing cell death. Cell death was recognized morphologically using the video record (Fig. 3A). We observed cell death at various stages of the cell lifetime. Some cells underwent cell death immediately after cytokinesis or, interestingly, at the

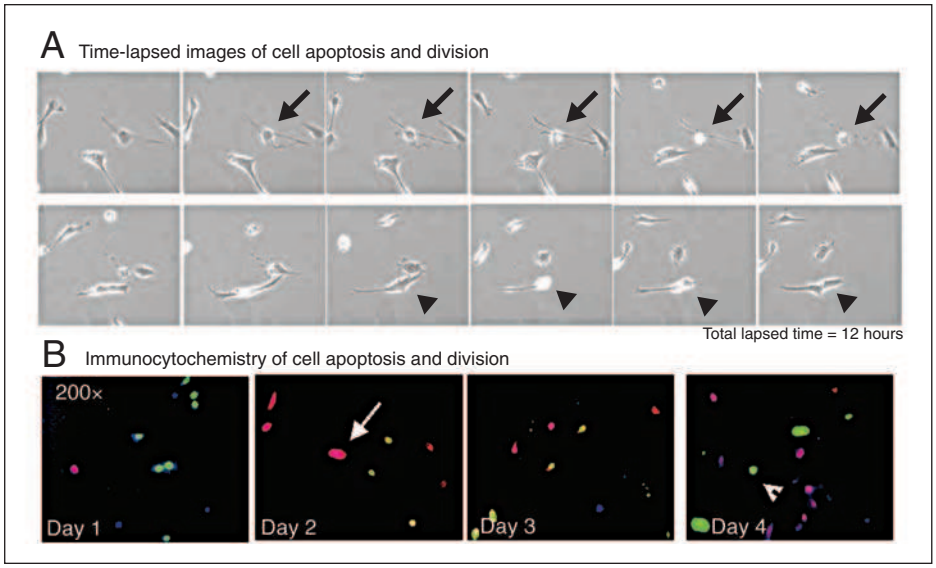

Figure 3. A) Time-lapsed video demonstrating visualization and morphological recognition of cell death (arrows) of MDSCs treated with actinomycin D. *Cell division is also visible (arrowheads). Total time lapsed is 12 hours. B) Immunocytochemistry to co-stain proliferating cells (BrdU, green), apoptotic cells (caspase-3, red), and nonproliferating cells (Hoechst, blue). Magnification = 200×.*

Table 1. Comparison of model equation (2) with model equation (1)

	Model with cell loss term		Model without cell loss term	
	r^2	α	r^2	α
Replicate 1	0.935	0.45	0.849	0.39
Replicate 2	0.887	0.43	0.417	0.28
Replicate 3	0.874	0.47	0.55	0.30
mean ($p < 0.05$)		0.45		0.32

same time as an expected division cycle (i.e., when one sister cell underwent cytokinesis, the other died). It was also common for apoptotic or necrotic cells to persist for several hours or days before undergoing cell death. The video findings of cell death were supported by anti-caspase-3 immunocytochemistry (Fig. 3B) of the cells treated with AD. Co-staining of caspase-3 (red), BrdU (green), and nuclei (blue) revealed the presence of apoptotic cells, mitotically active cells, and nonmitotic cells in the population.

The growth data (N + M) were fit using nonlinear regression with model equation (2), and the α parameter was numerically estimated. As a measure of how well the model predicts the data, i.e., how well the independent variable (t) predicts the dependent (N+M) variable in this model, we observed a strong association, with coefficients of determination $r^2 = 0.874$, 0.887, and 0.935 ($p < 0.001$). The mean mitotic fraction of the three replicates was estimated to be 0.45 (Table 1). Figure 4 shows the data fit to the model accounting for cell loss [equation (2)] compared with data fit to the model without the cell loss term [equation (1)]. When the cell loss term is not included, the coefficients of determination range from $r^2 = 0.417$ to 0.849 and α is significantly underestimated as 0.32 ($p < 0.05$).

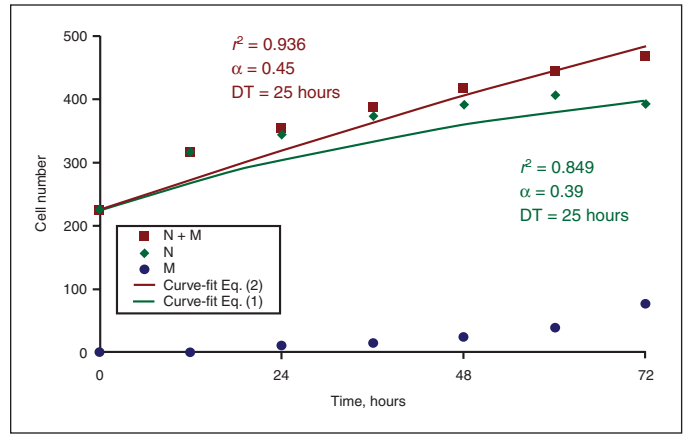

Figure 4. Curve-fit data. *Experimental data sets for MDSC growth with induced apoptosis are fit to the model equations using nonlinear regression. The results are* r^2 *coefficients and estimations of* α*, or dividing fraction. One representative replicate is shown here (rep 1). The normalized raw data are shown for the live cell count (N =* ◆*), the dead cell count (M =* ●*), and the total cell count (N+M =* ■*). Enumeration of cell loss yields a total cell count (N+M), which is higher than live cell count alone (N).* r^2 *values for N+M versus t (red curve) range from 0.87 to 0.94* (n = 3)*, with mean* α *= 0.45, in comparison to* r^2 *values for N versus t (green curve), which range from 0.42 to 0.85* (n = 3)*, with mean* α *= 0.32.*

Validation of Growth Model with Differentiation

Under low-serum and high-density conditions, a significant amount of terminal differentiation could be induced while still permitting symmetric divisions to mitotically active cells. Stem cell differentiation into the myogenic lineage was morphologically recognized based on myotube formation. The time-lapsed recordings revealed cell fusion activity (Fig. 5A), which subsequently was confirmed by the myogenic differentiation marker, myosin heavy chain (red), and Hoechst immunostaining (Fig. 5B). Mononuclear proliferating cells also were identifiable based on their BrdU-positive nuclei (green) (Fig. 5B).

The time-lapsed video was used to enumerate the terminally differentiated cells (nuclei), $N^{FusedNuclei}$, and the mononuclear cells, $N^{Mononuclear}$, at 12-hour time points, and these data then were fit to the growth model with differen-

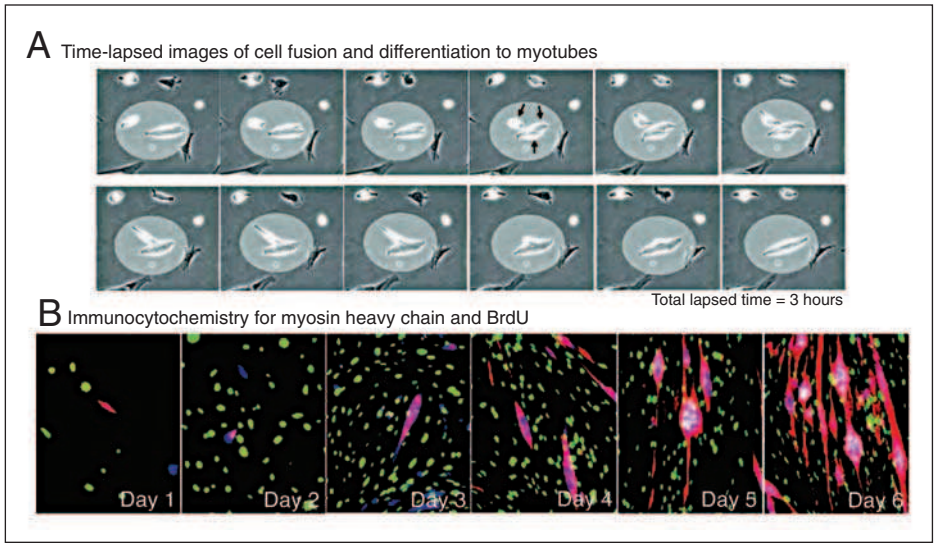

Figure 5. A) Time-lapsed video demonstrating visualization and morphological recognition of cell fusion and myogenic differentiation of MDSCs. *B) Immunocytochemistry of co-stained proliferating cells (BrdU, green), differentiated cells (myosin heavy chain, red), and nonproliferating cells (Hoechst, blue). Magnification = 200×.*

Table 2. Comparison of model equation (3) with model equation (1)

	Model with differentiation term		Model without differentiation term	
	r^2	α	r^2	α
Replicate 1	0.939	0.55	0.648	0.46
Replicate 2	0.816	0.63	0.598	0.58
Replicate 3	0.811	0.66	0.615	0.63
mean		0.61		0.56
($p < 0.05$)				

tiation [equation (3)]. The mitotic fraction was numerically estimated to be 0.60, and the coefficients of determination were 0.811, 0.816, and 0.939 ($p < 0.001$) (Table 2). Figure 6 displays the data prediction after model fitting and accounting for differentiation [equation (3.1)] compared with data prediction of the model without a differentiation term [equation (1)]. In the latter case, each myotube would be counted as only one cell. When cell differentiation is not included in the model, the coefficients of determination range from $r^2 = 0.598$ to 0.648 and the mean α parameter is estimated as 0.61, which is significantly different than the estimate from equation (3) ($p < 0.05$) (Table 2).

Discussion

The heterogeneity of stem cell populations is an issue that impacts all facets of stem cell research, from isolation to cell-cell signaling pathways to mathematical modeling. The simple, user-friendly models presented here can be utilized to assess parameters of heterogeneous cell population growth. In addition, they may serve as a framework for more complex models incorporating terms to account for interactions among subpopulations. Taken to the clinical setting, these models may serve as predictive tools to estimate the expansion time required to go from cell biopsy to cell transplantation.

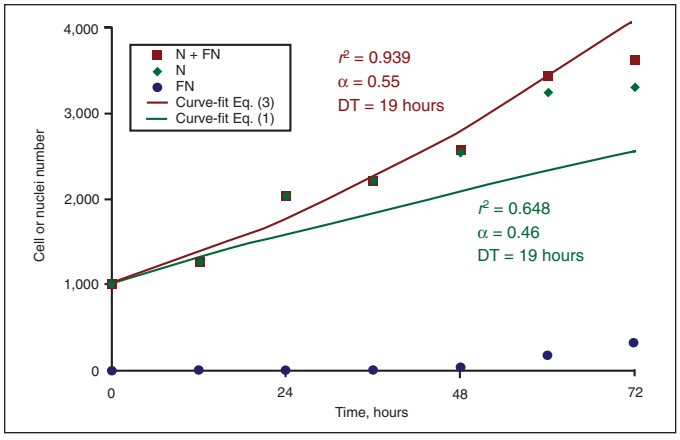

Figure 6. Curve-fit data. *Experimental data sets for MDSC growth with myogenic differentiation are fit to the model using nonlinear regression. One representative replicate is shown here (rep 1). The normalized raw data are shown for the live cell count (N = ◆), the differentiated cell or fused nuclei count (FN = ●), and the total cell count (N+FN = ■). Accounting for cellular fusion results in a total cell count (N+FN =* $N^{Mononuclear} + N^{FusedNuclei}$*), which is higher than individual cell count alone (N).* r^2 *values for* $N^{Mononuclear} + N^{FusedNuclei}$ *versus t (red curve) range from 0.81 to 0.94 (n = 3), with mean α = 0.61, in comparison to* r^2 *values for N versus t (green curve), which range from 0.62 to 0.65 (n = 3), with mean α = 0.56.*

One key assumption of the *Sherley* model, which we tested here, was that DT is constant. It is widely recognized that cell density affects cell behavior and phenotype, a belief that has led researchers to use standard culturing ranges under which a specific cell type is grown. For MDSCs, this confluency range is 10%-50% [40]. We observed that the DT remains relatively constant within this range. Although the appropriate statistical tests indicate that these parameters do not change significantly, the data show that there is a tendency toward an increase in the cell cycle time as confluency increases to >50%. This trend explains, in part, the sigmoidal shape often observed in culture and generally attributed to space and nutrient depletion. We also found no or minimal refractory periods between passages. After re-plating, the cells adhered and resumed division within 4-6 hours, and DT returned to previous values. This observation suggests that the model obtained with parameters within the 10%-50% confluency range validly represents the expected long-term expansion of the cells.

It is also noteworthy that the model equation can be used in place of other BrdU equations (exponential-based equations) that traditionally have been used to estimate DT. Just as the experimental data were curve-fit to estimate α using known DT, equation (1) can be used to estimate DT when α is determined experimentally. Furthermore, the *Sherley* expansion equation may be rewritten to obtain a nonexponential expression for the population doubling time (PDT), another parameter frequently used to describe population growth:

$$\text{Population Doubling Time} = DT\left[\frac{\ln(6\alpha - 2)}{\ln(2\alpha)} - 1\right]$$

Here we observe that doubling time is now more accurately represented as a function of both α and DT. An α value equal to 1 yields the exponential expression of population doubling time (= ln2/k = DT). Under the conditions of this study, PDT is calculated to be 20 hours for expansion growth, 50 hours for growth with apoptosis, and 39 hours for growth with differentiation. (The authors would like to emphasize the distinction between PDT and DT, where PDT is a property of the population and DT is a property of the cell).

When expansion is accompanied by significant cell loss, the growth model must account for this occurrence. The addition of a cell loss term makes the equation applicable for use in studies of cell populations in which apoptosis is a key event, such as anticancer agent or embryonic tissue developmental studies. Even clonal populations quickly become unsynchronized (due to individual variations in DT) such that the population will contain cells that have reached their divisional limit before others, enter senescence, and undergo programmed cell death [43]. If the rate of cell death is high, a measurement of the population growth must account for this cell loss. We treated cells with the transcription inhibitor AD to induce apoptosis, and then analyzed the fitness of the model. We observed an increase in the correlation coefficient as compared with the *Sherley* model or the exponential equation. Additionally, this system enabled assessment of other growth parameters, namely the division time and mitotic fraction, from which we can begin to understand the mechanism of action of given agents. For example, in the presence of AD, the number of apoptotic cells increased as expected; however, we also found that the remaining live cells had longer division time and decreased mitotic fraction. In the presence of 0.5 ng/ml AD, 45% of the daughter cells continued to divide actively with a DT equal to 21 hours; this population could recover when AD was removed.

We observed an even stronger model correlation when examining the cell growth of primary stem cell populations in which natural cell death occurred following fresh isolation ($r^2 = 0.967$, $\alpha = 0.44$, DT = 16 hours, data not shown). Notably, in this case and under many other conditions, the α and DT parameters may change over time, thus the concern for the time-scale on which the model is applied. After several weeks in culture, the primary MDSCs appeared to undergo some type of activation, and the mitotic fraction increased to ~70% (DT continued to be approximately 16 hours). The nondividing fraction of the cell population at this point appeared to comprise fewer apoptotic or necrotic cells and perhaps more cells moving toward terminal differentiation as the population matured in culture.

Indeed, one of the difficulties and focuses of stem cell research lies in controlling cell differentiation. While the promise of stem cell therapy is dependent upon the ability of these cells to undergo multilineage differentiation, actual therapies will require in vitro expansion of the undifferentiated phenotype. Our model includes terms that account for both the differentiated phenotype as well as the self-renewing phenotype. Therefore, the model can be used to assess the heterogeneity of a cell population and the growth kinetics resulting from the mixed subpopulations. In the case of MDSCs, terminal differentiation means that the cells fuse to become multinucleated myotubes. We again observed an increase in the correlation coefficient and an improved estimate of the mitotic fraction after incorporating a differentiation term. As compared with expansion conditions, we found that the differentiation medium and conditions led to a longer division time and a decreased mitotic fraction. Although we have not defined the self-renewing population phenotypically, we observed an actively dividing, nondifferentiated population that is likely responsible for giving rise to both the undifferentiated and the terminally differentiated populations. This model utilizes a mathematical approach to assess stem cell proliferation with attention to the various phenotypes resulting from alternative stem cell fates. While we have simplified the model to include the self-renewing and the terminally differentiated states, there are, in reality, several intermediate phenotypes that may have different rates of formation. While the estimate of the mitotic fraction is uniquely improved for the case of myogenic differentiation, the model could be applied in future studies to develop functions utilizing proliferation and differentiation rates based on the nonexponential model. Further, in the design of bioreactor systems, it may be more practical to enumerate cells rather than nuclei. In this way, fusion could be modeled as increases in M. It can be seen that in the case of cell fusion, the event is similar to cell loss, in that the cell or nucleus is no longer present in the population as a readily countable unit, nor is it contributing progeny to the population.

The models presented in this paper should facilitate the development of both a biological and mathematical understanding of stem cell dynamics and heterogeneity. These tools allow us to quantitatively assess parameters of stem cell population growth subject to both intrinsic and extrinsic regulation. An increased understanding of intercellular and microenvironmental determinants of stem cell fate teamed with appropriate growth models will allow for the development of bioreactor systems designed for the large-scale generation of phenotypically defined stem cells to be used in cellular therapy strategies.

Acknowledgments

The authors kindly thank *Dr. J.L. Sherley* for critical review of the manuscript, *Al Bahnson* and *Doug Koebler* of Automated Cell Technologies for assistance with the microscopic imaging system, and *Ryan Sauder* for careful editing. This work was supported by the Muscular Dystrophy Association, the National Institutes of Health (NIH R01 AR49684-01), and the William F. and Jean W. Donaldson Chair at Children's Hospital of Pittsburgh.

REFERENCES

1 Naughton GK. From lab bench to market: critical issues in tissue engineering. Ann N Y Acad Sci 2002;961:372-385.

2 Collins PC, Nielsen LK, Patel SD et al. Characterization of hematopoietic cell expansion, oxygen uptake, and glycolysis in a controlled, stirred-tank bioreactor system. Biotechnol Prog 1998;14:466-472.

3 Koller MR, Bradley MS, Palsson BO. Growth factor consumption and production in perfusion cultures of human bone marrow correlate with specific cell production. Exp Hematol 1995;23:1275-1283.

4 Madlambayan GJ, Rogers I, Casper RF et al. Controlling culture dynamics for the expansion of hematopoietic stem cells. J Hematother Stem Cell Res 2001;10:481-492.

5 Sherley JL. Asymmetric cell kinetics genes: the key to expansion of adult stem cells in culture. STEM CELLS 2002;20:561-572.

6 Qian X, Goderie SK, Shen Q et al. Intrinsic programs of patterned cell lineages in isolated vertebrate CNS ventricular zone cells. Development 1998;125:3143-3152.

7 Zhong W, Jiang MM, Weinmaster G et al. Differential expression of mammalian Numb, Numblike and Notch1 suggests distinct roles during mouse cortical neurogenesis. Development 1997;124:1887-1897.

8 Jan YN, Jan LY. Asymmetric cell division. Nature 1998;392:775-778.

9 Watt FM, Hogan BL. Out of Eden: stem cells and their niches. Science 2000;287:1427-1430.

10 Hackney JA, Charbord P, Brunk BP et al. A molecular profile of a hematopoietic stem cell niche. Proc Natl Acad Sci USA 2002;99:13061-13066.

11 Punzel M, Wissink SD, Miller JS et al. The myeloid-lymphoid initiating cell (ML-IC) assay assesses the fate of multipotent human progenitors in vitro. Blood 1999;93:3750-3756.

12 Kiger AA, White-Cooper H, Fuller MT. Somatic support cells restrict germline stem cell self-renewal and promote differentiation. Nature 2000;407:750-754.

13 Spradling A, Drummond-Barbosa D, Kai T. Stem cells find their niche. Nature 2001;414:98-104.

14 Baker FL, Sanger LJ, Rodgers RW et al. Cell proliferation kinetics of normal and tumour tissue in vitro: quiescent reproductive cells and the cycling reproductive fraction. Cell Prolif 1995;28:1-15.

15 Skehan P, Friedman SJ. Non-exponential growth by mammalian cells in culture. Cell Tissue Kinet 1984;17:335-343.

16 Mackey MC, Dormer P. Continuous maturation of proliferating erythroid precursors. Cell Tissue Kinet 1982;15:381-392.

17 Smith JR, Whitney RG. Intraclonal variation in proliferative potential of human diploid fibroblasts: stochastic mechanism for cellular aging. Science 1980;207:82-84.

18 Leblond C. Classifications of cell populations on the basis of their proliferative behavior. NCI Monog 1964;14:119-150.

19 Morris VB, Cowan R. A growth curve of cell numbers in the neural retina of embryonic chicks. Cell Tissue Kinet 1984;17:199-208.

20 Steel G. Growth kinetics of tumours: cell population kinetics in relation to the growth and treatment of cancer. Oxford: Clarendon Press, 1977.

21 Solyanik GI, Berezetskaya NM, Bulkiewicz RI et al. Different growth patterns of a cancer cell population as a function of its starting growth characteristics: analysis by mathematical modelling. Cell Prolif 1995;28:263-278.

22 Skehan P, Friedman SJ. Deceleratory growth by a rat glial tumor line in culture. Cancer Res 1982;42:1636-1640.

23 Fidler IJ, Hart IR. Biological diversity in metastatic neoplasms: origins and implications. Science 1982;217:998-1003.

24 Burton AC. Rate of growth of solid tumours as a problem of diffusion. Growth 1966;30:157-176.

25 Summers WC. Dynamics of tumor growth: a mathematical model. Growth 1966,30:333-338.

26 Gyllenberg M, Webb GF. A nonlinear structured population model of tumor growth with quiescence. J Math Biol 1990;28:671-694.

27 Gyllenberg M, Webb GF. Quiescence as an explanation of Gompertzian tumor growth. Growth Dev Aging 1989;53:25-33.

28 Izquierdo JM, Perez C. A stochastic approach for the interpretation of single pulse experiments in morphological multicompartments of renewing and exponentially growing cell populations. J Theor Biol 1983;101:39-75.

29 Voit EO. Cell cycles and growth laws: the CCC model. J Theor Biol 1985;114:589-599.

30 Cowan R, Morris VB. Cell population dynamics during the differentiative phase of tissue development. J Theor Biol 1986;122:205-224.

31 Cowan R, Morris VB. Determination of proliferative parameters from growth curves. Cell Tissue Kinet 1987;20:153-159.

32 Jones RB, Smith JR. A stochastic model of cellular senescence. II. Concordance with experimental data. J Theor Biol 1982;96:443-460.

33 Hirsch HR. Influence of the existence of a resting state on the decay of synchronization in cell culture. J Theor Biol 1984;111:61-79.

34 Bergman MO. Mathematical model for contact inhibited cell division. J Theor Biol 1983;102:375-386.

35 Sherley JL, Stadler PB, Stadler JS. A quantitative method for the analysis of mammalian cell proliferation in culture in terms of dividing and non-dividing cells. Cell Prolif 1995;28:137-144.

36 Deasy BM, Qu-Peterson Z, Greenberger JS et al. Mechanisms of muscle stem cell expansion with cytokines. STEM CELLS 2002;20:50-60.

37 Jankowski RJ, Deasy BM, Cao B et al. The role of CD34 expression and cellular fusion in the regeneration capacity of myogenic progenitor cells. J Cell Sci 2002;115:4361-4374.

38 Qu Z, Balkir L, van Deutekom JC et al. Development of approaches to improve cell survival in myoblast transfer therapy. J Cell Biol 1998;142:1257-1267.

39 Lee JY, Qu-Petersen Z, Cao B et al. Clonal isolation of muscle-derived cells capable of enhancing muscle regeneration and bone healing. J Cell Biol 2000;150:1085-1100.

40 Qu-Petersen Z, Deasy B, Jankowski R et al. Identification of a novel population of muscle stem cells in mice: potential for muscle regeneration. J Cell Biol 2002;157:851-864.

41 Aoyama T, Takemura G, Maruyama R et al. Molecular mechanisms of non-apoptosis by Fas stimulation alone versus apoptosis with an additional actinomycin D in cultured cardiomyocytes. Cardiovasc Res 2002;55:787-798.

42 Yamazaki Y, Tsuruga M, Zhou D et al. Cytoskeletal disruption accelerates caspase-3 activation and alters the intracellular membrane reorganization in DNA damage-induced apoptosis. Exp Cell Res 2000;259:64-78.

43 Linskens MH, Harley CB, West MD et al. Replicative senescence and cell death. Science 1995;267:17.